SMC-TR-94-22

AEROSPACE REPORT NO.
TR-93(3925)-6

AD-A279 253

Atomic Velocity Distributions
in a Hydrogen Beam Effusing Out
of an RF Discharge Dissociator

15 March 1994

Prepared by

B. JADUSZLIWER and Y. C. CHAN
Electronics Technology Center
Technology Operations

DTIC
ELECTE
MAY 1 3 1994
S B D

Engineering and Technology Group

DTIC QUALITY INSPECTED 3

94-14334

THE AEROSPACE
CORPORATION

94 5 12 0 44

Wm. Kyle Sneddon, Captain USAF
Deputy, Industrial & International Division
Plans and Programs Directorate
Phillips Laboratory

REPORT DOCUMENTATION PAGE

1. AGENCY USE ONLY (Leave blank)	2. REPORT DATE 15 March 1994	3. REPORT TYPE AND DATES COVERED

4. TITLE AND SUBTITLE
Atomic Velocity Distributions in a Hydrogen Beam Effusing Out of an RF Discharge Dissociator

5. FUNDING NUMBERS
F04701-88-C-0089

6. AUTHOR(S)
Jaduszliwer, B. and Chan, Y. C.

7. PERFORMING ORGANIZATION NAME(S) AND ADDRESS(ES)
The Aerospace Corporation
Technology Operations
El Segundo, CA 90245-4691

8. PERFORMING ORGANIZATION REPORT NUMBER
TR-93(3925)-6

9. SPONSORING/MONITORING AGENCY NAME(S) AND ADDRESS(ES)
Space and Missile Systems Center
Air Force Materiel Command
2430 E. El Segundo Boulevard
Los Angeles Air Force Base, CA 90245

10. SPONSORING/MONITORING AGENCY REPORT NUMBER
SMC-TR-94-22

11. SUPPLEMENTARY NOTES

12a. DISTRIBUTION/AVAILABILITY STATEMENT
Approved for public release; distribution unlimited

12b. DISTRIBUTION CODE

13. ABSTRACT (Maximum 200 words)

We have measured atomic hydrogen velocity distributions in an effusive beam coming out of an rf discharge dissociator by using a magnetic deflection technique. Dissociator pressures varied between 0.028 and 0.340 torr. At low dissociator pressures, the measured atomic velocity distributions were narrower than the expected beam-Maxwellians; at higher pressures, they were indistinguishable from beam-Maxwellians at the dissociator wall temperature, indicating full thermalization of the atoms prior to exiting the dissociator. Monte Carlo simulations of the thermalization process within the dissociator reproduce these results and point out the important role of vibrational excitation of the background hydrogen molecules as an energy loss mechanism. Our results are significant when designing magnetic state selectors for spin- or hyperfine-polarized atomic hydrogen beams.

14. SUBJECT TERMS
Hydrogen masers, Hydrogen dissociators, Hydrogen beams

15. NUMBER OF PAGES
22

16. PRICE CODE

17. SECURITY CLASSIFICATION OF REPORT UNCLASSIFIED	18. SECURITY CLASSIFICATION OF THIS PAGE UNCLASSIFIED	19. SECURITY CLASSIFICATION OF ABSTRACT UNCLASSIFIED	20. LIMITATION OF ABSTRACT

Preface

1

Contents

Figures

I. INTRODUCTION

A radio frequency (rf) discharge dissociator is the most frequently used source of atomic hydrogen. Hydrogen masers, the time and frequency standards of choice whenever the highest possible frequency stability is required, use an rf dissociator followed by a hexapole or quadrupole magnet to focus a beam of state-selected hydrogen atoms at the entrance orifice of the maser bulb.[1] Similar combinations of rf discharge dissociators and state-selecting, focusing magnets have been used to produce beams of spin-polarized hydrogen atoms used in atomic, nuclear, and high-energy physics experiments.[2,3] Since atomic trajectories within a hexapole or quadrupole magnet will depend strongly on atomic velocities, such magnets also act as fairly narrow-band velocity filters.[4] Efficient use of the state-selected atomic hydrogen source, which becomes a paramount consideration when designing hydrogen masers qualified for space flight, requires a good match between the velocity distribution of the hydrogen atoms exiting the dissociator and the velocity bandpass of the state-selecting magnet.

In many instances, the tacit assumption is made that the atoms exiting the dissociator will be in thermal equilibrium with the dissociator wall; this assumption is not necessarily valid. Dissociation of molecular hydrogen in an rf discharge takes place after spin-exchange collisions with energetic discharge electrons.[5] The ground state of the H_2 molecule has a $^1\Sigma_g$ configuration; the lowest energy triplet state is the repulsive $^3\Sigma_u$, which has the same asymptotic dissociation limit as the ground state at about 4.5 eV, and which also will be the endpoint of any radiative cascade starting after excitation of a higher triplet level. Thus, any spin-exchange collision will end up dissociating the molecule. Since the threshold energy for excitation of the $^3\Sigma_u$ state is 8.8 eV,[6] after dissociation, each one of the hydrogen atoms will carry away more than 2 eV of excess energy. Depending on dissociator geometry and gas density, the hydrogen atoms may or may not undergo enough gas and wall collisions to thermalize fully before they exit.

Relatively little is actually known about the velocity distribution of hydrogen atoms effusing out of rf discharge dissociators. Walraven and Silvera[7] have studied the characteristics of a beam of hydrogen atoms produced in a microwave discharge followed by a cryogenic thermal accommodator and found the velocity distribution to be Maxwellian at the accommodator temperature. Hershcovitch et al.[8] studied a similar dissociator-accommodator combination operated at higher pressures and flow rates and measured velocity distributions in reasonable agreement with the results of supersonic flow-regime calculations. These results show that accommodators can thermalize the hydrogen beam, but they are not directly applicable to the problem under study since thermal accommodators are not commonly used in hydrogen masers or polarized hydrogen beam sources. Miller[9] investigated a helium-cooled microwave discharge dissociator at relatively high pressure (3.3 torr) and measured a velocity distribution that was slightly narrower than a beam-Maxwellian at the estimated discharge temperature.

We have determined velocity distributions of atomic-hydrogen beams effusing out of an rf discharge dissociator having a geometry and operating parameters similar to those of a maser dissociator by analyzing the deflection of the atomic trajectories in an inhomogeneous magnetic field. These distributions are presented and compared with the results of Monte Carlo simulations of the atomic hydrogen thermalization process within the dissociator bulb.

II. EXPERIMENTAL TECHNIQUE

Atomic hydrogen velocity distributions have been determined using a magnetic deflection technique. Figure 1 shows schematically our experimental arrangement. Hydrogen is fed through a standard temperature-controlled Pd-Ag leak[10] into a cylindrical double-walled Pyrex bulb 15-cm long with a 1.9-cm internal diameter and a 3.8-cm external diameter. Compressed air flows between the internal and external walls to provide cooling, and rf power is coupled inductively to the discharge by an external 25-turn coil. The hydrogen beam exits the dissociator through a 0.025-cm-wide, 0.1-cm-high slit, is collimated by a second 0.025-cm-wide slit set at d = 63.7 cm away from the dissociator slit, and then travels between the polepieces of an L = 11.4-cm-long, inhomogeneous-field electromagnet, configured in the "two-wire" geometry described by Rabi *et al*[11]. After additional travel through a D = 71.3 cm drift tube, the beam is detected by an rf quadrupole mass analyzer. The dissociator is attached to the rest of the apparatus by a flexible vacuum bellows, and can be displaced transversely by micrometer screws, allowing measurement of the angular distribution of atoms deflected by the inhomogeneous magnetic field.

The atomic fraction in the hydrogen beam, φ, was measured using the quadrupole mass analyzer. The results were corrected for the H^+ fraction when detecting H_2; typically, values between 0.65 and almost 1.00 were obtained, depending on total dissociator pressure and rf power coupled to the discharge. The dissociator pressure was measured using a capacitance manometer, and injected and reflected rf power were monitored continuously as indicators of the steady-state character of the discharge.
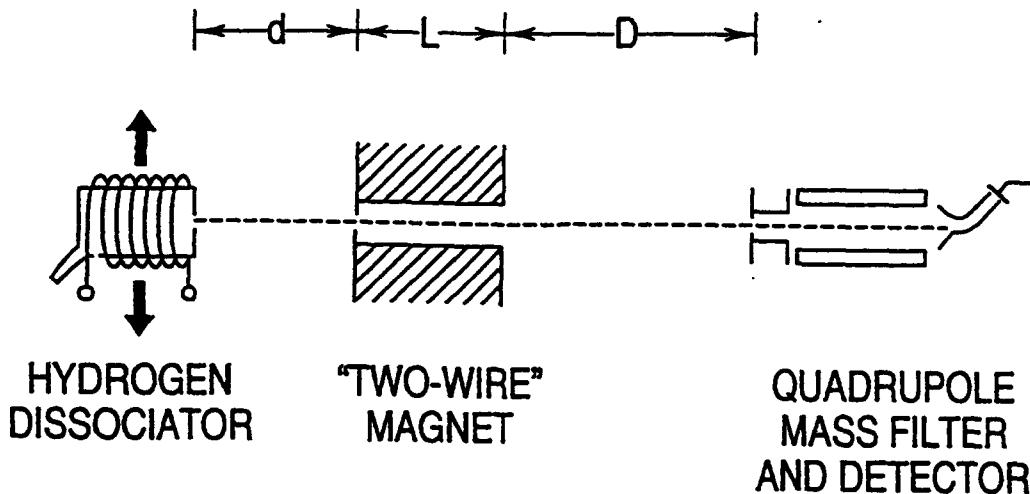
Figure 1.   Schematic representation of the experimental arrangement.

An atom having magnetic moment, μ, immersed in a magnetic field, B, has energy, $E = -\mu \cdot B$. The force acting on the atom is $F = grad(\mu \cdot B) \approx \mu_{eff} grad(B)$, where μ_{eff} is the component of the atomic magnetic moment along the direction of the field. In general, μ_{eff} will depend on the atomic ground-state quantum numbers and the field strength. For an atom having total electron angular momentum and nuclear spin quantum numbers $J = 1/2$ and I, respectively, and total azimuthal quantum number, M, the effective magnetic moment, is given by Breit-Rabi's formula[12],

$$\mu_{eff} = \pm \frac{\varepsilon + 2M/(2I+1)}{[1 + 4M\varepsilon/(2I+1) + \varepsilon^2]^{1/2}} \mu_0, \tag{1}$$

where the (+) sign corresponds to the total angular momentum quantum number, $F = I-1/2$, and the (-) sign to $F = I+1/2$. The parameter $\varepsilon = g\mu_0 B/\Delta W$, where g is the atomic Lande factor, ΔW is the atomic hyperfine splitting, and μ_0 is the Bohr magneton.

Figure 2 shows the cross section of the "two-wire" magnet; 2α is the separation between the "equivalent wires."[13] If a narrow atomic beam enters the magnet at $x = 1.2\alpha$ (as determined by a collimating slit), and the atomic transversal displacements within the magnet are small, the force acting on the atoms remains approximately constant,[14] and so does the acceleration:
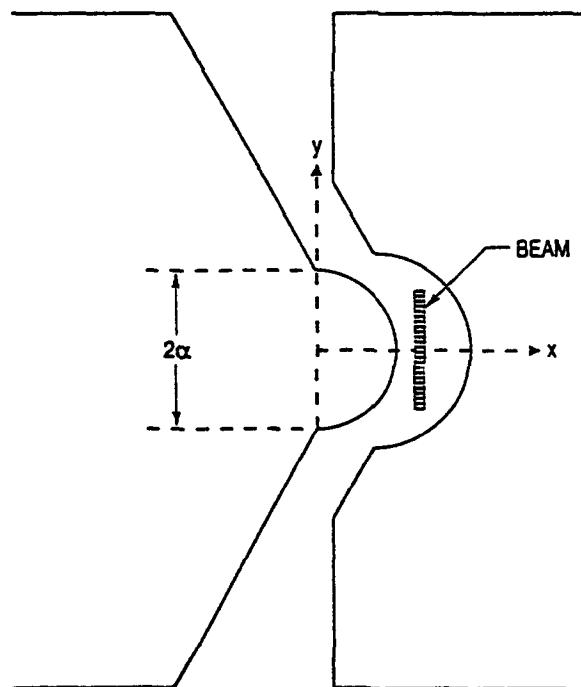
Figure 2. Cross section of the "two-wire" magnet polepieces.

$$a = \frac{0.984}{\alpha} \frac{\mu_{eff}B}{m} \mathbf{i}, \qquad (2)$$

where B is the magnetic field strength at the atomic beam, m is the mass of the atom, and $\mathbf{i}$ a unit vector along the x (deflection) axis. Under these conditions, the trajectory equations for the atoms traveling from source to detector can be solved easily. With no magnetic field applied, an atom of effective magnetic moment μ_{eff} and speed v leaving the source slit at x_S will be detected at $x_D = -x_S(L+D)/d$. If now a magnetic field B is applied, and the detector is not moved, an identical atom will have to leave the plane of the source slit at x_S', given by

$$x_{S'} = x_S + \frac{a}{v^2} \frac{Ld}{2} \left(1 + \frac{D}{L+D}\right) \qquad (3)$$

in order to be detected at x_D. If $f_0(x_S)$ is the distribution of detected atoms as a function of source-slit position at zero field, and g(v) is the speed distribution of atoms leaving the source slit, the distribution of detected atoms at non-zero field vs. source-slit position, $f(x_S)$, will be given by

$$f(x_S) = \sum_{F,M} \int_0^{\infty} f_0(x_S - K_{FM}/v^2) g(v) dv, \qquad (4)$$

where

$$K_{FM} = \frac{0.492}{\alpha} \frac{\mu_{eff}BLd}{m} \left(1 + \frac{d}{L+D}\right). \qquad (5)$$

Both $f_0(x_S)$ and $f(x_S)$ can be measured, and then Eq. (4) can be used to verify whether a model velocity distribution, g(v), is consistent with the measured deflected atom distribution.

III. CALIBRATION AND VERIFICATION EXPERIMENT

A preliminary experiment involving the use of a rubidium atomic beam was performed in order to calibrate the electromagnet and test the use of Eq. (4) to verify a model velocity distribution. A two-chambered effusive oven of standard design[15] was installed at the end of the source bellows, where the rf dissociator would normally be located.

As shown by Eq. (1), an atom will have $\mu_{eff} = 0$ for B such that $\epsilon = -2M/(2I+1)$. At field intensities determined by

$$B = \frac{-M}{2I+1} \frac{\Delta W}{\mu_0}$$

(6)

atoms with M < 0 will not be deflected by the inhomogeneous field in the magnet. Natural rubidium is a mixture of 72.2% [85]Rb (I = 5/2) and 27.8% [87]Rb (I = 3/2). [85]Rb has zero effective moments at B = 361G (M = -1) and B = 722G (M = -2), while [87]Rb has zero effective moments at B = 1221G (M = -1). Figure 3 shows the detected atomic-beam signal as a function of magnet-coil current, with the rubidium beam source on the apparatus axis. At the field values listed
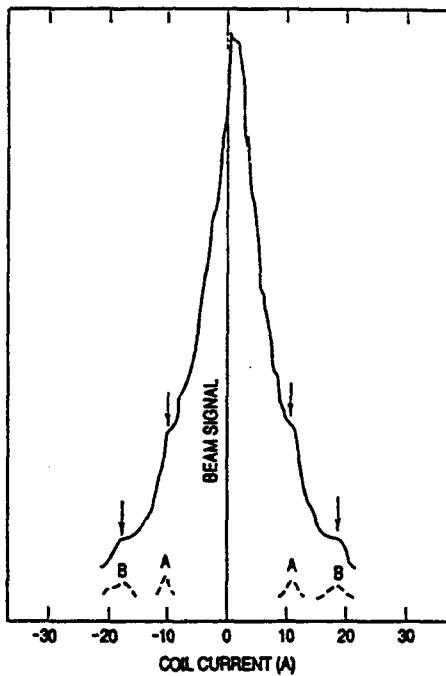

Figure 3. Rubidium atomic-beam signal (oven and detector on axis) vs. magnet-coil current. Arrow shows features due to zero effective moment states. Dashed lines were obtained by subtracting the local constant-slope background from each feature. A: Rb_{85}, M =-2; B: Rb_{87}, M =-1.

above, atoms in the $\mu_{eff} = 0$ states will travel through the "two-wire" magnet without deflection, leading to an increased detector signal. The effect of the zero effective moment states can be made more apparent in Figure 3 by subtracting from each one of the marked features of the local sloping background. The peaks labeled A and B can be identified with the zero effective moments at 722G and 1221G, respectively, yielding a calibration of 66.3G/A for the "two-wire" magnet.

The rubidium atomic beam-speed distribution was assumed to be beam-Maxwellian,

$$g(v) = (2/\beta) (v/\beta)^3 \exp[-(v/\beta)^2], \tag{7}$$

where $\beta = (2kT/m)^{1/2}$, and $T = 484$ K, the absolute oven temperature. We measured $f_0(x_S)$ and $f(x_S)$, and then used Eq. (4), with the proper statistical weight for each rubidium isotope, to calculate the expected $f(x_S)$;

$$f(x_S) = 0.722f_{85}(x_S) + 0.278f_{87}(x_S). \tag{8}$$

Figure 4 shows measured and calculated deflected-atom distributions at $B = 1061$G. For $x_S < 0$ the agreement between measured and calculated $f(x_S)$ is excellent; these results, showing that the rubidium beam-speed distribution was indeed a source-temperature beam-Maxwellian, validate our experimental technique. The agreement is poorer for $x_S > 0$; this is the convex polepiece side of the magnet, and atoms may be traveling too close to it. Thus, only the $x_S < 0$ side of the deflection pattern was considered when evaluating model-speed distributions for the atomic-hydrogen beam.
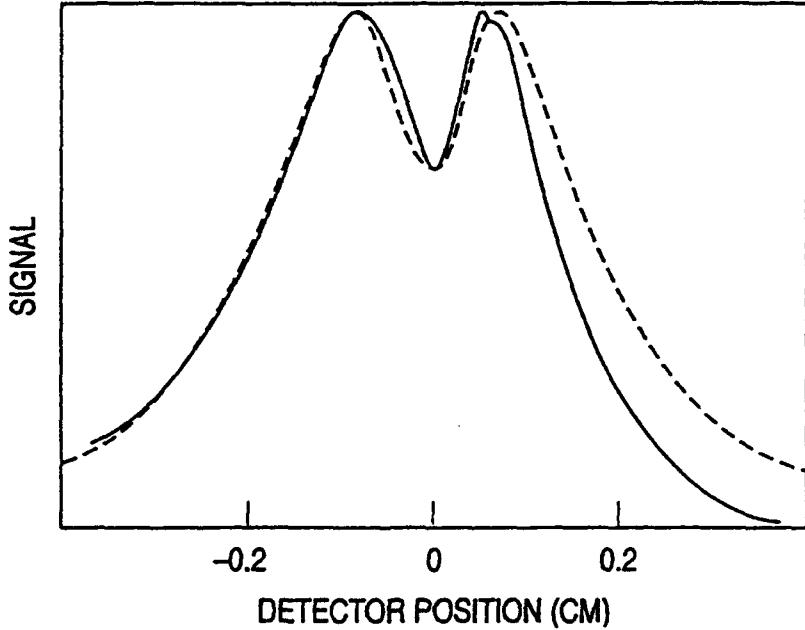

Figure 4. Distribution of deflected rubidium atoms at B = 1061 Gauss. Full line: measured distribution. Dashed line: distribution calculated assuming a beam-Maxwellian atomic-speed distribution.

12

IV. ATOMIC HYDROGEN DEFLECTION MEASUREMENTS

Since the focus of this study was on the degree of thermalization of the atomic-hydrogen beam effusing out of the dissociator, we used our magnetic deflection technique to investigate the dependence of the atomic-hydrogen speed distributions on dissociator pressure. Deflection profiles $f(x_S)$ were measured at $B = 995G$ (corresponding to 15 A excitation current) for total dissociator pressures between 28 and 340 mtorr. Undeflected (zero-field) beam profiles, $f_0(x_S)$, and atomic-hydrogen beam fractions, φ, were also measured in each case.

Under free molecular flow conditions, $f_0(x_S)$ should be fully determined by the source and collimator slits, and be independent of source pressure. This was indeed the case for the range of dissociator pressures we have explored, as shown in Figure 5. The line in the figure shows $f_0(x_S)$ calculated for our geometry assuming a trapezoidal beam intensity distribution[16] folded with a detector of finite width; the calculation contains no free parameters and is in excellent agreement with the measurements. The slight discrepancies at the top (scans proceeding from left to right)
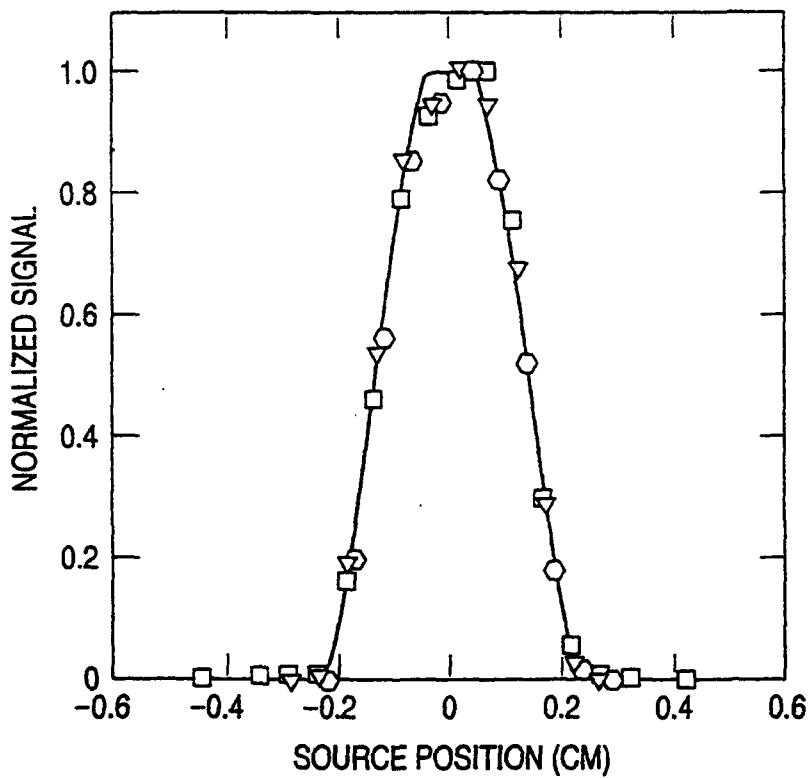

Figure 5. Atomic-hydrogen beam profile (zero deflecting magnetic field). Squares: measurements at 319 mtorr. Triangles: measurements at 215 mtorr. Hexagons: measurements at 58 mtorr. Full line: calculated beam profile.

13

are due to detection system response/recovery times which were comparable to source point-dwell-times. We believe the calculated $f_0(x_S)$ to be a better description of the undeflected beam than any of our measurements; thus, it was used with Eq. (4) to calculate deflected beam distributions.

Deflected beam profiles were calculated using

$$f(x_S) \approx \varphi f_1(x_S) + (1-\varphi)f_0(x_S) \ , \tag{9}$$

where the first term describes the deflected atomic-hydrogen beam profile, with $f_1(x_S)$ computed using Eq. (4), and the second term represents the contribution of the H_2 fraction of the beam, which is not deflected by the magnet. We performed a non-linear, least-squares fit to the $x_S < 0$ deflection data using Eq. (9), with a beam-Maxwellian, $g(v)$, Eq. (7), and β as a free parameter. Figure 6(a) shows the results for $p = 319$ mtorr. The left lobe of the best fitting $f(x_S)$, obtained for $\beta \approx 2.29 \times 10^3$ m/s and indicated by the full line, is in quite good agreement with the measured deflected beam data, indicating that thermalization of the hydrogen atoms within the dissociator bulb is essentially completed. The equilibrium temperature derived from the best value of β is 318 K. The results of the fits at lower dissociator pressures, on the other hand, strongly suggest incomplete thermalization. Figure 6(b) shows measured and best-fitting deflected-beam profiles for $p = 28$ mtorr. Inspection of the left lobe of the beam profile shows that the $f(x_S)$ calculated using the beam-Maxwellian, $g(v)$, indicated by the full line, predicts too many atoms undergoing very small as well as very large deflections. Since atomic deflections $\Delta x_S \propto 1/v^2$, this suggests that the low- and high-speed tails of the beam-Maxwellian speed distribution are substantially higher than those of the actual atomic-hydrogen beam-speed distribution at low dissociator pressure. Similar results are shown in Figure 6(c) for $p = 86$ mtorr.

In order to evaluate the differences between the actual atomic-hydrogen beam-speed distribution and the beam-Maxwellian distribution, which would be characteristic of a fully thermalized atomic-hydrogen beam, we used the model distribution

$$g(v) = C_N v^3 \exp[-(v-v_0)^2/2\sigma^2], \tag{10}$$

where v_0 and σ are treated as free parameters in a non-linear, least-squares fitting procedure. C_N is a normalization factor, and $g(v)$ becomes beam-Maxwellian in the limit $v_0 = 0$, in which case $\beta = \sqrt{2}\sigma$. Best-fitting deflected-beam profiles, $f(x_S)$, obtained using that model distribution are shown in Figure 6 by the dashed lines. The results at 319 mtorr are comparable to those obtained with the beam-Maxwellian distribution, but at the lower pressures, 28 and 86 mtorr, they are in much better agreement with the measured deflection profiles.

The model speed distributions obtained using Eq. (10) with the best-fitting values of v_0 and σ for $p = 319, 28$, and 86 mtorr are shown in Figures 7(a), (b), and (c), respectively, together with the corresponding best-fitting beam-Maxwellians. As expected from the previous discussion, at the lower pressures, the best-fitting model distributions are significantly narrower than the beam

14

Maxwellian; at higher pressures, the two become indistinguishable, indicating full thermalization of the atomic-hydrogen beam.
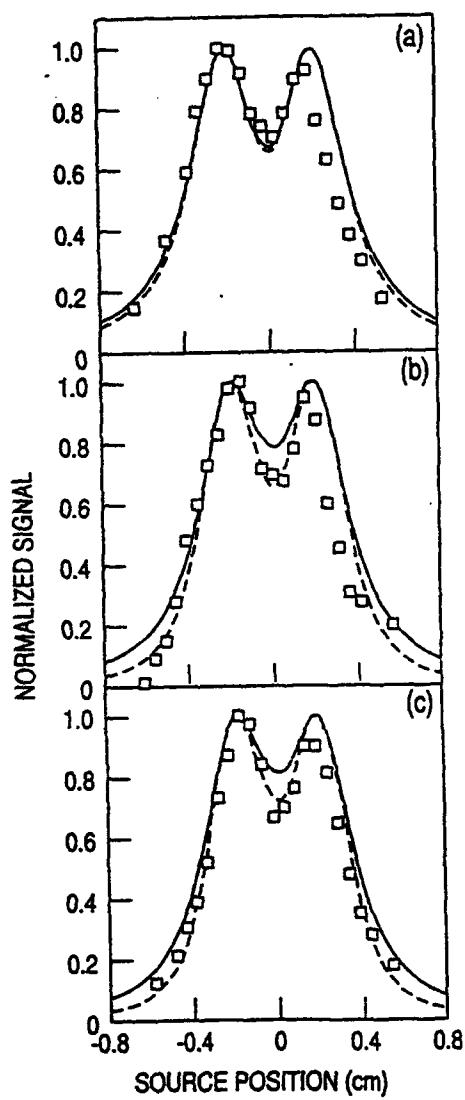
Figure 6. Distribution of deflected hydrogen atoms at B = 995 Gauss. Squares: measurements. Full lines: calculations using the best-fitting beam-Maxwellians. Dashed lines: calculations using two-parameter model speed distributions. (a) p = 319 mtorr; (b) p = 28 mtorr; (c) p = 86 mtorr.
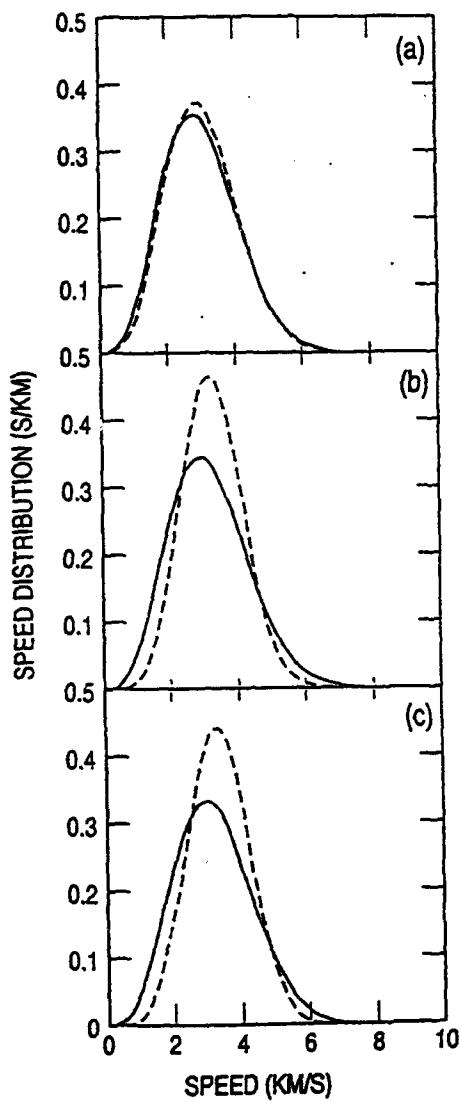
Figure 7. Atomic-hydrogen speed distributions giving best fits to the magnetic-deflection data. Full lines: beam-Maxwellian distributions. Dashed lines: two-parameter model distributions. (a) p = 319 mtorr; (b) p = 28 mtorr; (c) p = 86 mtorr.

15

V. THERMALIZATION PROCESS SIMULATIONS

The low-pressure results presented in the preceding section confront us with an apparent paradox: since the atomic beam-speed distribution is non-Maxwellian, the hydrogen atoms in the beam must leave the dissociator bulb without undergoing enough collisions to thermalize fully, but, at the same time, they must undergo enough collisions to drop from an initial energy of more than 2 eV (as discussed in Section I) to the 0.05 eV characteristic of the measured speed distributions. These seemingly contradictory requirements can be satisfied simultaneously in the presence of a process having a significant collision cross section and a large energy loss per event; impact vibrational excitation of the H_2 molecules present in the dissociator (a loss of about 0.52 eV/collision[17]) is a likely candidate, allowing the kinetic energy of the hydrogen atoms to drop to very low values in about four such collisions, well before a fully thermal distribution can be developed. In order to provide qualitative support for this interpretation of the speed distributions inferred for low dissociator pressures, we developed a computer code to perform Monte Carlo, two-dimensional simulations of the thermalization of hydrogen atoms produced by dissociation of $^3\Sigma_u$ H_2 molecules.

In our simulations, hydrogen atoms with an initial kinetic energy of 2.15 eV are born at random positions within a two-dimensional rectangular enclosure having an exit aperture. The enclosure and aperture dimensions are those of our dissociator. The atoms are followed as they travel within the enclosure, colliding with other hydrogen atoms, hydrogen molecules, or the enclosure walls. Energy is exchanged in elastic collisions with hydrogen atoms or molecules, inelastic (rotational or vibrational) collisions with the molecules, or thermal accommodation at the enclosure walls. Each atom is followed until it exits through the aperture or recombines on the enclosure boundary. If the atom exits the enclosure within the atomic beam acceptance angle, the count in the appropriate speed bin in the atomic beam-speed distribution is incremented by one. The simulation stops after a preset number of beam atoms have been counted. The input parameters are the wall temperature, the total hydrogen pressure, the hydrogen dissociation fraction, the cross sections for (H,H) and (H,H_2) elastic collisions as well as (H,H_2) vibrational and rotational excitations, and the average thermal accommodation coefficient in collisions with the wall. The output of the simulation is a statistical sampling of the atomic-hydrogen beam-speed distribution, integrated over 400-m/s-width speed bins.

The simulations were performed for a two-dimensional gas in order to shorten the computation time as much as possible, but they incorporate all of the relevant physical processes. The results obtained for 300, 30, and 90 mtorr are shown in Figures 8(a), (b), and (c), respectively. The beam-Maxwellian speed-distribution characteristic of a two-dimensional gas,

$$g(v) = \frac{4}{\sqrt{\pi}\beta}(v/\beta)^2 \exp[-(v/\beta)^2],\tag{11}$$

17
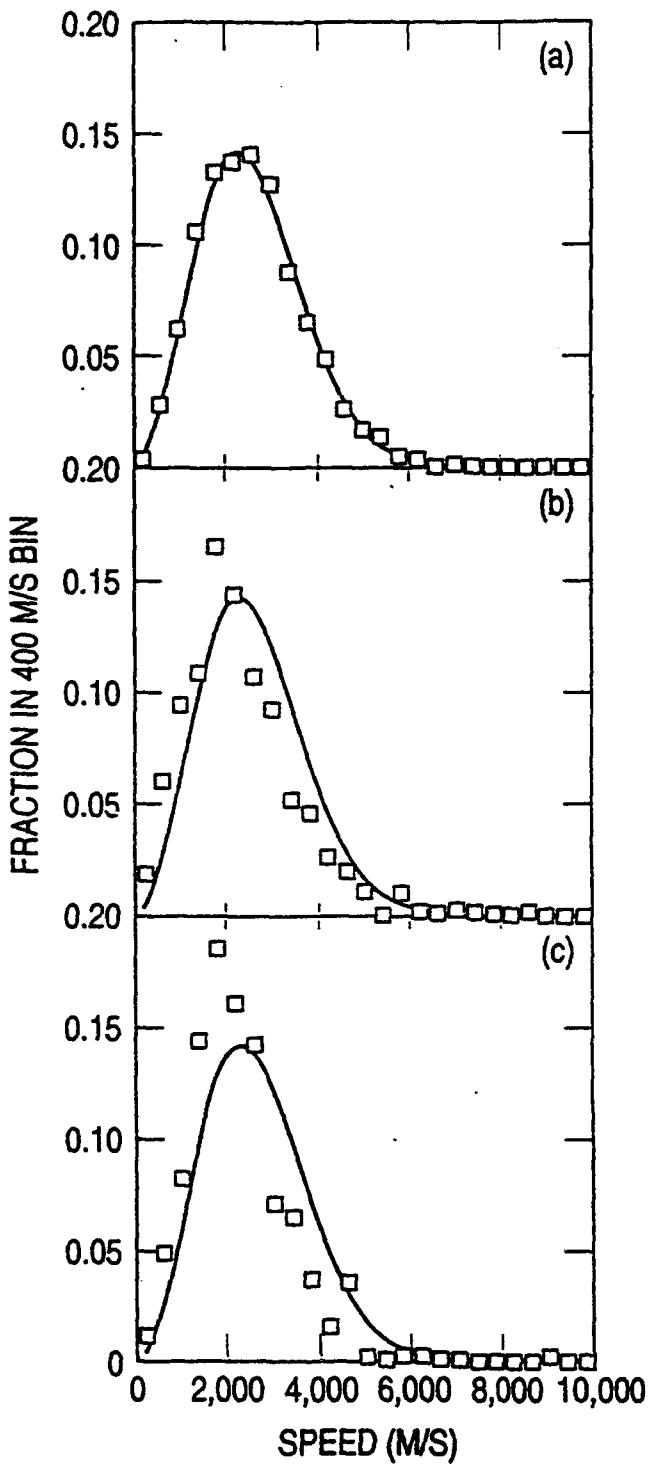
Figure 8. Atomic-hydrogen speed distributions for a two-dimensional gas, integrated over the width of a 400-m/s speed bin. Squares: Monte Carlo simulation results. Full lines: beam-Maxwellians at the 320 K wall temperature. (a) p = 300 mtorr; (b) p = 30 mtorr; (c) p = 90 mtorr.

calculated at the dissociator wall temperature, T ≈ 320 K, and integrated over the 400-m/s speed-bin width, is also shown in each figure for comparison purposes. At the two lower pressures, the simulation results are significantly narrower than the two-dimensional beam Maxwellian. At 300 mtorr, the simulation results are in excellent agreement with the two-dimensional beam Maxwellian (allowing for the statistical spread characteristic of the results of a Monte Carlo calculation), indicating a completely thermalized atomic-hydrogen beam. These results are fully consistent with our experimental determinations of atomic-hydrogen beam-speed distributions. If the vibrational excitation energy loss mechanism is "turned off" in the simulation by assigning a very small value to the corresponding cross section, very different results are obtained for low pressures, as illustrated in Figure 9. The flat, fast-atom tail, caused by the lack of an efficient energy loss mechanism, would show up in the magnetic-deflection measureme   tained for low dissociator pressures as a significant signal excess near beam axis; no such   s is observed in Figures 6(b) and (c).
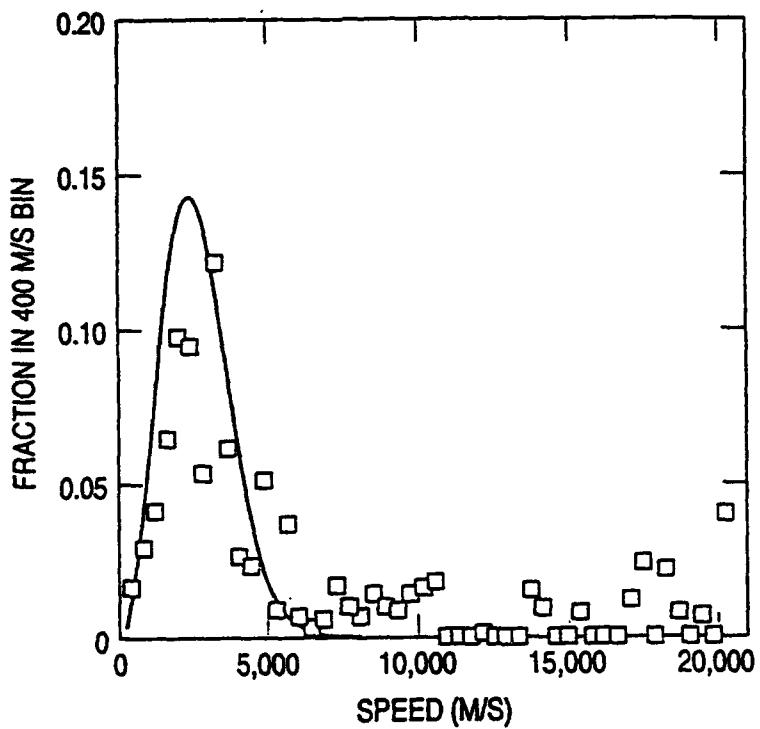

Figure 9.   Atomic-hydrogen speed distributions for a two-dimensional gas, integrated over the width of a 400-m/s speed bin. Squares: Monte Carlo simulation results at 30 mtorr dissociator pressure, with (H,H₂) impact vibrational excitation disallowed. Full line: beam-Maxwellian at 320 K wall temperature.

VI. CONCLUSIONS

The results of this study show that the Maxwellian character of the velocity distribution in an atomic-hydrogen beam effusing out of an rf discharge dissociator cannot be taken for granted. Full thermalization will always be achieved for high enough dissociator pressures, but when operating at low dissociator pressures, non-thermal speed distributions may obtain. Of course, what pressure constitutes a "low" pressure will be determined in each case by the dissociator geometry. The unavoidable presence of some molecular hydrogen within the dissociator bulb makes the escape of high-energy atoms very unlikely since impact vibrational excitation of H_2 provides a very efficient energy-loss mechanism; thus, at low pressures, the atomic-speed distribution lacks any significant "hot-atom" tails that might be expected otherwise. The speed distributions that we have inferred from our magnetic-deflection measurements have averages that are quite close to thermal, but at low dissociator pressures, they are significantly narrower than beam-Maxwellians.

21

REFERENCES

1. D. Kleppner, H. M. Goldenberg, and N. F. Ramsey, *Phys. Rev.* 126, 603 (1962).

2. D. M. Crowe, X. Q. Guo, M. S. Lubell, J. Slevin, and M. Eminyan, *J. Phys. B* 23, L325 (1990).

3. R. Keller, L. Dick, and M. Fidecaro, *Helv. Phys. Acta Suppl.* 6, 48 (1961).

4. H. M. Brash, D. M. Campbell, P. S. Farago, A. G. A. Rae, H. C. Siegmann, and J. S. Wylkes, *Proc. R. Soc. Edinburgh, Sect. A* 68, 159 (1968/69, Part II).

5. S. J. B. Corrigan and A. von Engel, *Proc. R. Soc. (London) A* 245, 335 (1958).

6. S. J. B. Corrigan, *J. Chem. Phys.* 43, 4381 (1965).

7. J. T. M. Walraven and I. F. Silvera, *Rev. Sci. Instrum.* 53, 1167 (1982).

8. A. Hershcovitch, A. Kponou, and T. O. Niinikoski, *Rev. Sci. Instrum.* 58, 547 (1987).

9. T. M. Miller, *J. Appl. Phys.* 45, 1713 (1973).

10. J. Viennet, P. Petit, and C. Audoin, *J. Phys. E.* 6, 261 (1973).

11. I. I. Rabi, J. M. B. Kellogg, and J. R. Zacharias, *Phys. Rev.* 46, 157 (1934).

12. G. Breit and I. I. Rabi, *Phys. Rev.* 38, 2082 (1931).

13. N. F. Ramsey, *Molecular beams*, (Oxford University Press, New York, 1956), p. 400.

14. N. F. Ramsey, ibid., p. 398.

15. N. F. Ramsey, ibid., p. 364.

16. N. F. Ramsey, ibid., p. 16.

17. M. D. Harmony, *A Physicist's Desk Reference*, (H. L. Anderson, Ed., AIP, New York, 1989), p. 239.

TECHNOLOGY OPERATIONS

The Aerospace Corporation functions as an "architect-engineer" for national security programs, specializing in advanced military space systems. The Corporation's Technology Operations supports the effective and timely development and operation of national security systems through scientific research and the application of advanced technology. Vital to the success of the Corporation is the technical staff's wide-ranging expertise and its ability to stay abreast of new technological developments and program support issues associated with rapidly evolving space systems. Contributing capabilities are provided by these individual Technology Centers:

Electronics Technology Center: Microelectronics, solid-state device physics, VLSI reliability, compound semiconductors, radiation hardening, data storage technologies, infrared detector devices and testing; electro-optics, quantum electronics, solid-state lasers, optical propagation and communications; cw and pulsed chemical laser development, optical resonators, beam control, atmospheric propagation, and laser effects and countermeasures; atomic frequency standards, applied laser spectroscopy, laser chemistry, laser optoelectronics, phase conjugation and coherent imaging, solar cell physics, battery electrochemistry, battery testing and evaluation.

Mechanics and Materials Technology Center: Evaluation and characterization of new materials: metals, alloys, ceramics, polymers and their composites, and new forms of carbon; development and analysis of thin films and deposition techniques; nondestructive evaluation, component failure analysis and reliability; fracture mechanics and stress corrosion; development and evaluation of hardened components; analysis and evaluation of materials at cryogenic and elevated temperatures; launch vehicle and reentry fluid mechanics, heat transfer and flight dynamics; chemical and electric propulsion; spacecraft structural mechanics, spacecraft survivability and vulnerability assessment; contamination, thermal and structural control; high temperature thermomechanics, gas kinetics and radiation; lubrication and surface phenomena.

Space and Environment Technology Center: Magnetospheric, auroral and cosmic ray physics, wave-particle interactions, magnetospheric plasma waves; atmospheric and ionospheric physics, density and composition of the upper atmosphere, remote sensing using atmospheric radiation; solar physics, infrared astronomy, infrared signature analysis; effects of solar activity, magnetic storms and nuclear explosions on the earth's atmosphere, ionosphere and magnetosphere; effects of electromagnetic and particulate radiations on space systems; space instrumentation; propellant chemistry, chemical dynamics, environmental chemistry, trace detection; atmospheric chemical reactions, atmospheric optics, light scattering, state-specific chemical reactions and radiative signatures of missile plumes, and sensor out-of-field-of-view rejection.